



Hybrid Gels via Bulk Interfacial Complexation of Supramolecular Polymers and Polyelectrolytes

Journal:	<i>Soft Matter</i>
Manuscript ID	SM-ART-01-2021-000168.R1
Article Type:	Paper
Date Submitted by the Author:	25-Mar-2021
Complete List of Authors:	Cotey, Thomas; Northwestern University Sai, Hiroaki; Northwestern University, Center for Bioinspired Energy Science Perez, Cynthia; Northwestern University Palmer, Liam; Simpson Querrey Institute for BioNanotechnology , ; Northwestern University, Stupp, Samuel; Northwestern University,

Hybrid Gels via Bulk Interfacial Complexation of Supramolecular Polymers and Polyelectrolytes

Thomas J. Cotey,¹ Hiroaki Sai,^{2,5} Cynthia Perez,¹ Liam C. Palmer,^{2,3,5} and Samuel I. Stupp^{1,2,3,4,5,6}

¹ Department of Materials Science and Engineering, Northwestern University, Evanston, Illinois 60208, United States

² Center for Bio-Inspired Energy Science, Northwestern University, Evanston, Illinois 60208, United States

³ Department of Chemistry, Northwestern University, Evanston, Illinois 60208, United States

⁴ Department of Medicine, Northwestern University, Chicago, Illinois 60611, United States

⁵ Simpson Querrey Institute, Northwestern University, Chicago, Illinois 60611, United States

⁶ Department of Biomedical Engineering, Northwestern University, Evanston, Illinois 60208, United States

Abstract

Hierarchical self-assembly leading to organized supramolecular structures across multiple length scales has been of great recent interest. Earlier work from our laboratory reported the complexation of peptide amphiphile (PA) supramolecular polymers with oppositely charged polyelectrolytes into a single solid membrane at a macroscopic interface. We report here the formation of bulk gels with many internal interfaces between the covalent and supramolecular polymer components formed by the rapid chaotic mixing of solutions, one containing negatively charged PA nanofibers and the other the positively charged biopolymer chitosan. We found that formation of a contact layer at the interface of the solutions locks the formation of hydrogels with lamellar microstructure. The nanofiber morphology of the supramolecular polymer is essential to this process since gels do not form when solutions of supramolecular assemblies form spherical micelles. We found that rheological properties of the gels can be tuned by changing the relative amounts of each component. Furthermore, both positively and negatively

charged proteins are easily encapsulated within the contact layer of the gel, which provides an interesting biomedical function for these systems.

Introduction

The mixing of oppositely charged polyelectrolytes in aqueous solution resulting in associative phase separation with polymer-rich phases is referred to as polyelectrolyte complexation.¹ These polymer-rich phases are known as polyelectrolyte complexes (PECs) and can take the form of films,²⁻⁴ micelles,^{5,6} gels,^{7,8} solutions,^{1,9} or precipitates.¹⁰ PECs are prevalent in nature, such as in membrane-less organelles^{11,12} and also have applications in tissue engineering^{13,14} and drug delivery.^{3,15,16} An obvious benefit of using polyelectrolyte complexes for biomedical applications is their spontaneous formation without requiring catalysts or initiators required in hydrogels that form through chemical reactions.¹⁷ Most research of PECs focuses on interactions between covalent polymers, and complexation between covalent and supramolecular polymers remains relatively unexplored.

Self-assembly offers a path to create dynamic and responsive hierarchical materials with applications including regenerative medicine,^{18,19} drug delivery,²⁰ and biosensing.²¹ Peptide amphiphiles (PAs) are composed of amino acid sequences that have been modified with a hydrophobic moiety to promote their self-assembly.²²⁻²⁴ The Stupp Laboratory has developed PA nanostructures based on the competition between strong β -sheet hydrogen bonding and a charged region that promotes solubility.^{23,25-28} In water, hydrophobic collapse due to the aliphatic tail and β -sheet formation induce assembly of the molecules into one-dimensional supramolecular nanostructures.^{22,23,25} These PA nanostructures have shown the ability to bind growth factors and

amplify signaling, which could enable future therapies that incorporate proteins.^{29,30} The PA nanofibers have highly charged surfaces and can be gelled with multivalent ions.^{31–33}

The Stupp Laboratory previously reported the formation of hierarchical membranes and closed sacs formed with the negatively charged polymer hyaluronic acid (HA), and the positively charged PA $C_{16}V_3A_3K_3$.³⁴ Due the electrostatic interactions between the negatively charged HA and positively charged $C_{16}V_3A_3K_3$, a contact layer formed at the interface of the two solutions which lead to self-assembly of PA nanofibers at the interface. The HA then diffused through the contact layer into the PA compartment, nucleating self-assembly of PA fibers perpendicular to the contact layer, which in turn lead to growth of PA-HA membrane.³⁴ Subsequent works explored the physical properties^{35,36} of these membranes as well as their ability to be used for anti-cancer therapeutics³⁷ and promote angiogenesis.³⁸ In these examples, the two solutions were put in contact without mixing, resulting in a single, complexed interface. More recently, oppositely charged PA-polymer systems have been reported in the formation of layer-by-layer films,³⁹ hydrogels that develop without the formation of a contact layer,⁴⁰ printed toroidal structures,⁴¹ and systems that undergo morphogenesis during membrane formation due to conformational changes of the polymer.⁴² These examples involve bringing the solutions in contact without further mixing. We investigate here the formation of bulk gels through interfacial complexation between negatively charged PA and the positively charged polymer chitosan utilizing combination of scanning electron microscopy, confocal microscopy, X-ray scattering, rheology, and absorbance spectroscopy. Since hydrogels have been reported to aid delivery of proteins,^{43,44} we also explore the hypothesis that the emergent structure could promote encapsulation, localization, and retention of proteins within the hydrogel.

Results and Discussion

Chitosan is a water soluble positively charged polysaccharide derived from chitin which is biodegradable, biocompatible, and previous work has investigated its use as a biomaterial for wound dressings.^{17,45,46} Gels were produced using 1 wt% solutions of chitosan and PA with the sequence C₁₆V₃A₃E₃-OH (E3OH), which has its peptide chain terminated by a carboxylic acid group. The two solutions were added simultaneously to opposite sides of a glass vial, followed immediately by mixing with a vortex agitator, resulting in the rapid formation of a gel within chitosan rich excess fluid (Fig. 1). As shown in Fig. 2A-C, scanning electron micrographs of the resulting gels revealed a sheet-like morphology with fibrous textures. The structure of PA nanofibers is retained in the final gel, as shown by X-ray scattering experiments (Fig. 2D). These sheets approach millimeter length scales in width and are micrometers thick.

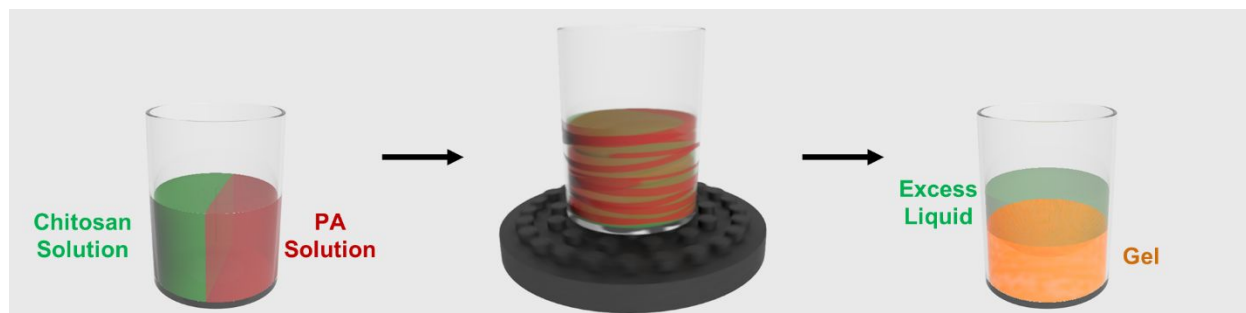


Fig. 1 Schematic representation of gel formation by adding PA and chitosan solutions to opposite sides of a vial followed by immediate mixing.

Since electron microscopy cannot determine the distribution of PA and chitosan molecules, confocal laser scanning microscopy was used to explore these domains using specific fluorescent labels on each molecule. The chitosan polymer was labeled with fluorescein isothiocyanate (FITC), and PA molecules labeled with 5-carboxytetramethylrhodamine (TAMRA) (see Electronic Supplementary Information). By using different dye labels for each component, it was possible to determine the extent of colocalization of both components versus separation into

distinct morphologies. In the E3OH-chitosan polyelectrolytic complex, we see a clear distinction between the chitosan and the PA domains (see Fig. 2E). Based on confocal micrographs, the PA component of the gel appears to be encapsulated by a layer of chitosan. By obtaining a z-stack in confocal microscopy, it is possible to explore the three-dimensional structure of the material. The confocal z-stack imaging (Fig. 2F) indeed confirmed the morphology observed by SEM. The gel is made up of sheets that are crumpled and folded over each other, and they contain PA nanofibers in their interior encased by chitosan outer layers. Similar structures were also observed when mixing was performed with a dual-barrel syringe with a mixing tip (ESI Fig. S1).

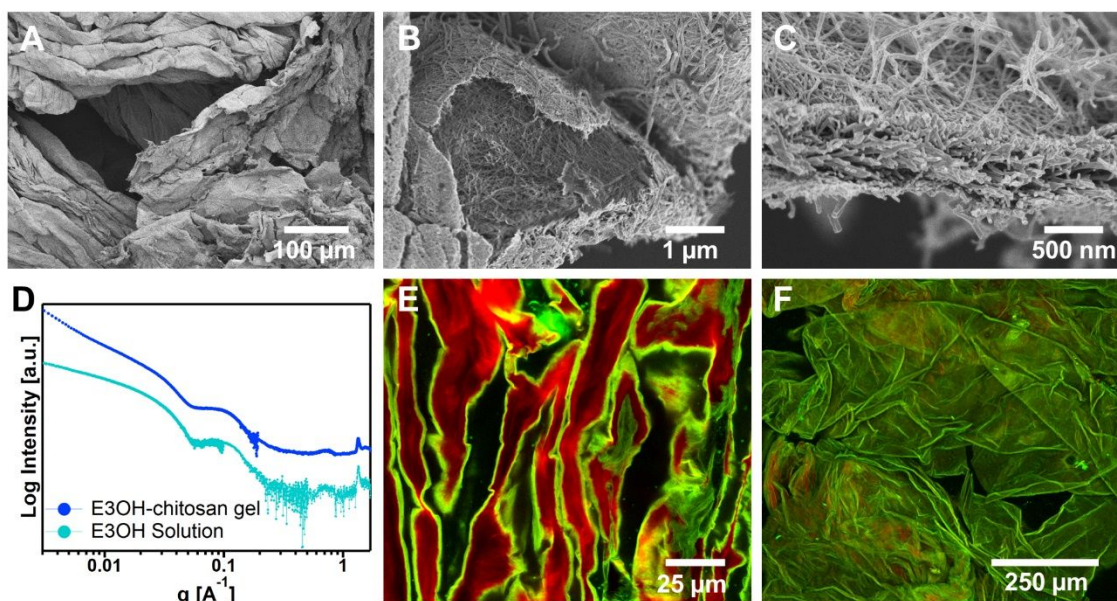


Fig. 2 (A-C) Scanning electron micrographs of critical point dried E3OH-chitosan gels at various magnifications. (D) Small, medium, and wide-angle x-ray scattering of E3OH-chitosan gel and an E3OH solution. (E) Confocal micrograph of a gel cross section revealing the presence of PA (red channel) and chitosan (green channel). (F) Maximum intensity projection of a z-stack Confocal micrograph with PA channel in red and chitosan channel in green.

Chaotic mixing of both components is characterized by the generation of increasing amounts of interfacial area between them as well as the development of a lamellar fluid structure^{47–49} as shown schematically in the first transformation of Fig. 3. The deformations that fluids experience during chaotic mixing are commonly referred to as “stretching and folding,” and the amount of

interfacial area generated is related to the amount of stretching experienced by the fluid elements.^{47,48} If the fluids are miscible, extensive mixing eventually results in the formation of a homogeneous phase. During the mixing of chitosan and the oppositely charged PA, we observed complexation at the interfaces of the two fluids, locking in the striations that make up the lamellar structure of the mixing fluids as depicted schematically in Fig. 3. As a result, the rapid interfacial gelation leads to nonequilibrium, sheet-like structures composed of both PA and chitosan. Scanning electron microscopy and confocal microscopy confirmed the lamellar structure of the gel and showed that our material was heterogeneous in terms of dimensions of the sheets as well as their random orientation relative to each other, which we hypothesize is a result of the chaotic manner in which the two solutions were mixed.

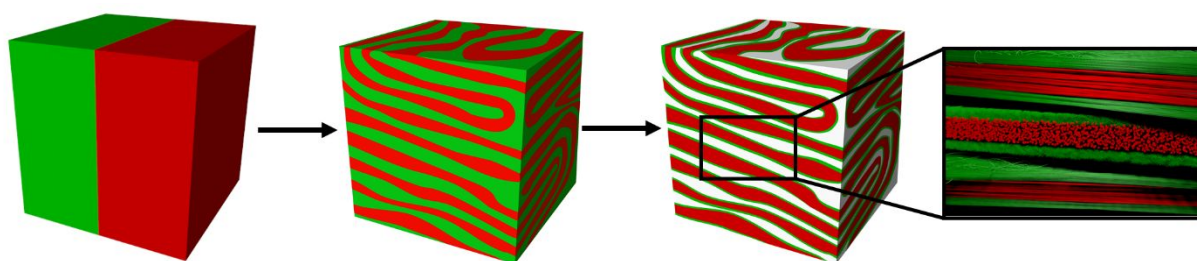


Fig. 3 Schematic representation of the morphology formed by the positively charged biopolymer chitosan (green) and an oppositely charged PA (red). Mixing leads to stretching and folding of the fluids and results in the formation of a material with many interfaces due to electrostatic complexation at their interfaces, which prevents further mixing and locks a nonequilibrium structure. The spaces between the lamellae, shown in white in the third cube and shaded in the zoomed inset, are composed of fluid in the final gel.

The ability of the mixed components to form gels was found to greatly depend on pH of the PA solutions as well as their concentration. Gel formation required fibrous PA solutions at neutral a pH, but PA solutions at high pH, which contain predominantly spherical micelles due to electrostatic repulsive interactions among PA molecules,^{50–52} lead to the formation of precipitates during complexation with chitosan (ESI Fig. S2). This result demonstrates the importance of the PA nanofiber morphology in the development of gels with fibrous sheet-like morphology. This

agrees well with previous work that found that spherical assemblies of PAs did not result in formation of a noticeable diffusion barrier or nanofiber growth when exposed to oppositely charged polyelectrolytes.⁵³

We also found that a sufficiently high PA concentration was required for gel formation. When the concentration of PA in solution was below 0.75 wt%, gel microparticles were obtained rather than a percolating network. This is likely because at lower PA concentration viscosity decreases and the striations become thinner and weaker, thus leading to tearing during rapid mixing. Because the sheets are smaller due to tearing, they were unable to make a cohesive network. On the other hand, at higher PA concentrations, we consistently observed sheet-like structures, and the formation of small particles was not observed (ESI Fig. S3). Additionally, sheet-like microstructures were observed regardless of rotation speed during vortex mixing (ESI Fig. S4). It was also found that the ratio of the polymer solution to the PA solution affects the mechanical properties of the gel. As shown in Fig. 4A, increasing the volume ratio of polymer solution used results in increased modulus and strain at break. A gel formed from a mixture of 1.5 wt% PA solution and 1 wt% chitosan solution in a 1:1 volume ratio has a storage modulus in the linear viscoelastic region that is approximately 2.4 times higher than a 3:1 mixing ratio and 4.8 times higher than a 5:1 mixing ratio. This is consistent with previous work that found that increasing the amount of polymer increased the modulus of planar PA-polymer membranes.³⁵

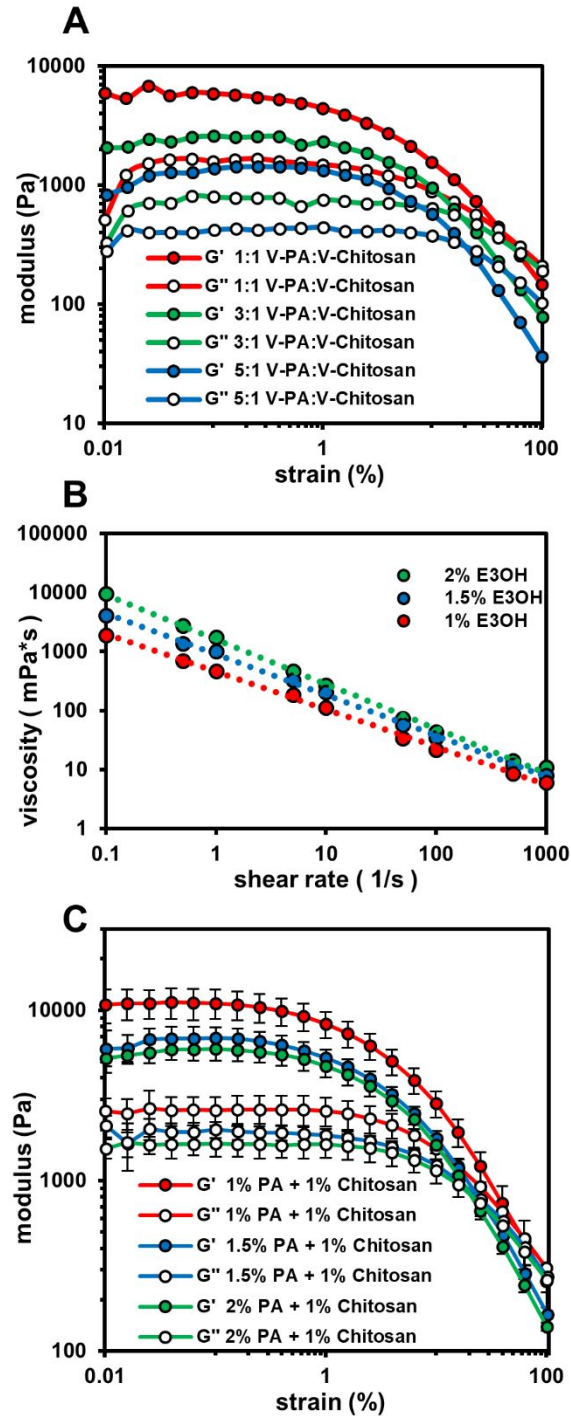


Fig. 4 (A) Oscillatory rheology amplitude sweeps of gels made by mixing solutions of 1.5 wt% PA with a 1 wt% chitosan solution in varied volume ratios. (B) Oscillatory amplitude sweep of gels prepared by mixing 1 wt% chitosan solution with an equal volume of PA solutions of varying concentration. (C) Viscosity of PA solutions as a function of concentration with power law fits that all have negative slopes indicating shear thinning behavior in all PA samples.

The mechanical properties of the hydrogels can also be tuned by varying the concentration of the PA solution while keeping the chitosan concentration constant. In these experiments, the chitosan solution used was 1 wt%, and the E3OH solution used was either 1 wt%, 1.5 wt%, or 2 wt% with constant volume ratios of both solutions (Fig. 4B). As the concentration of the PA solution increases from 1 wt% to 2 wt%, the storage moduli of the gels in the linear viscoelastic region decreases from approximately 10 kPa to 6 kPa, respectively. This was unexpected because gels typically show an increase in moduli with as the concentration of gelator increases. We hypothesize that this phenomenon is a result of how effective the mixing of the chitosan and PA solutions is as gelation takes place at the interfaces between both. Increasing the concentration of PA in solution from 1 wt% to 2 wt% increases the viscosity of the solution, with all of the PA solutions showing shear thinning behavior and higher concentrations consistently showing a higher viscosity for a given shear rate (Fig. 4C). This increase in viscosity lowers the amount of mixing that can occur before mixing is arrested by gelation at interfaces. Decreased mixing results in lower surface area, thus reducing interactions among sheets in the resultant gel. The shear moduli of the gels are highly dependent on the interactions between the surfaces of the sheets in the gels, so we assume that as proper mixing of the two solutions deteriorates, the moduli of gels decrease. To explore this hypothesis, we determined the composition of the gels by quantifying the amount of FITC-labeled chitosan in fluid excluded from the gels using absorbance spectroscopy. Absorbance spectroscopy shows that as the concentration of PA increases, we observe higher amounts of chitosan in the excluded fluid, corresponding to less chitosan in the gel (ESI Fig. S7B) as well as a lower ratio of chitosan to PA in the gel (ESI Fig. S7C). Increasing the amount of the negative component would not decrease the amount of the positive component that was complexed in a typical polyelectrolyte complex. However, in this

system, as the mixing efficiency is decreased due to increased viscosity, we expected to create lower moduli gels with less gelled interfacial area as suggested by rheometry and absorbance spectroscopy data.

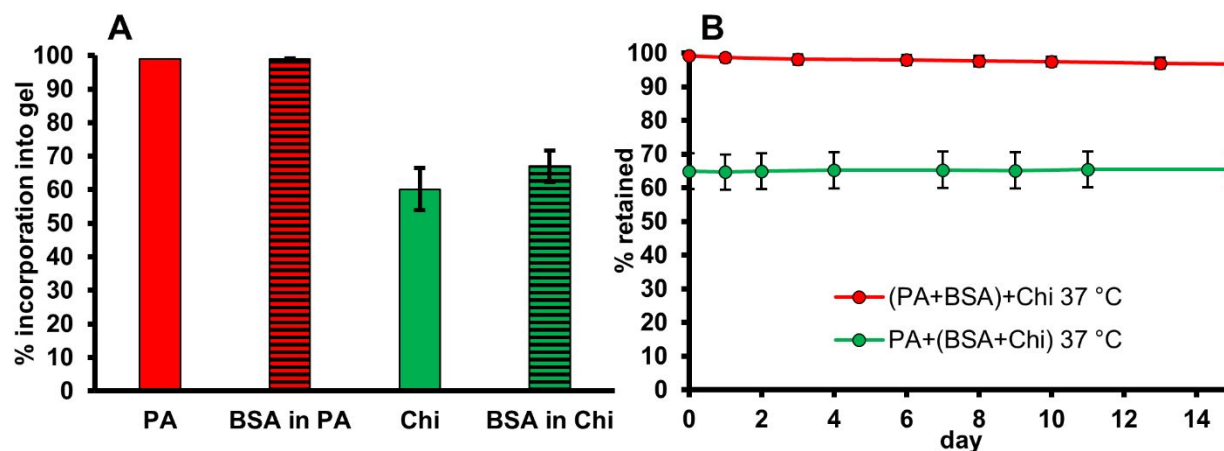


Fig. 5 (A) Graph of the amount of PA and chitosan that are incorporated into hydrogel during gelation as well as the amount of BSA that is incorporated when it is dissolved in either PA solution or chitosan solution prior to mixing. (B) Plot of BSA retention in hydrogels when placed in a PBS bath at 37 °C (BSA was dissolved in either PA solution (red) or chitosan solution (green) prior to gelation).

Because the PA solution is effectively encapsulated by the contact layer, we hypothesized that this gel would offer a platform for protein encapsulation and delivery. We explored this possibility using bovine serum albumin (BSA) labeled with FITC so that the release and encapsulation could be monitored. We found that encapsulation depended on which solution the protein was dissolved in prior to gel formation (Fig. 5A). The initial encapsulation efficiency was found to be 99% when the FITC-BSA was dissolved in the PA solution prior to mixing. However, the initial encapsulation efficiency was found to be $67 \pm 5\%$ when the FITC-BSA was dissolved in the chitosan solution prior to mixing. The higher encapsulation that occurs when the protein is dissolved in the PA solution is likely a result of the PA solution itself being nearly entirely incorporated into the gel. In contrast, only $60 \pm 6\%$ of the chitosan is incorporated into the gel. Because a significant amount of the chitosan solution is not incorporated into the gel, it

is not surprising that a corresponding amount of protein that was in the chitosan solution is also not incorporated into the gel.

In addition to measuring the encapsulation of the protein in E3OH-chitosan hydrogels, retention in the hydrogels was also measured (Fig. 5B). For this experiment, protein loaded hydrogels were produced by dissolving FITC-BSA in either the PA solution or the chitosan solution prior to gel formation during mixing. Gels were washed and then placed in PBS solutions at 37 °C, and the absorbance of FITC-BSA in the supernatant PBS solution was monitored over time. The amount of protein retained in the gels produced with BSA dissolved in the chitosan solution starts off lower because a relatively lower amount of FITC-BSA is encapsulated in these gels. In the gels produced with FITC-BSA dissolved in the chitosan solution, there was no significant release detected over the course of 15 days, resulting in a $65 \pm 5\%$ retention. In gels produced with FITC-BSA dissolved in the PA solution prior to gel formation, after 15 days, $97 \pm 0.5\%$ of the protein was retained. While it is difficult to make a direct comparison, the retention of BSA in these gels appears to be higher than previously reported PA-polymer gels that do not have a diffusion barrier.⁴⁰ We hypothesize that the slower protein release observed is due to the dense diffusion barrier at the polymer-PA interface.

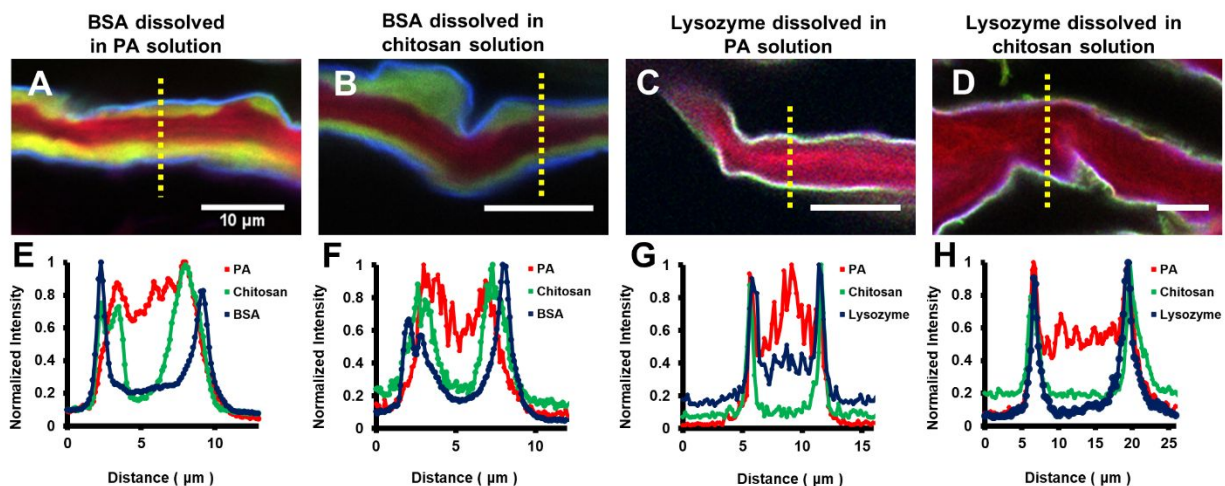


Fig. 6 (A-D) Confocal micrographs of PA-chitosan gels containing either Alexa Fluor 647-labeled BSA or Alexa Fluor 647 labeled lysozyme (FITC chitosan in green, TAMRA-E3 in red, and BSA or lysozyme in blue) all scale bars 10 micrometers. (E-H) Plots of the normalized intensity values of each channel (FITC chitosan in green, TAMRA-E3 in red, and Alexa Fluor 647 lysozyme in blue) for the line cut (yellow dashed line) of the composite confocal image above each respective plot.

Confocal experiments were performed to determine where BSA was located in gels (Fig. 6 A,B,E,F). For these experiments, protein loaded hydrogels were produced by dissolving Alexa Fluor647 labeled BSA in either the PA solution (Fig. 6A and 6E) or the chitosan solution (Fig. 6B and 6F) prior to gel formation during mixing. In both experiments the FITC-chitosan and TAMRA-E3 were used so that all gel components could be studied. As shown in Fig. 6A and 6B, the Alexa Fluor 647 labeled BSA was found to have its highest concentration in the outermost region of the sheets, regardless of whether or not the BSA was dissolved in the PA solution or the chitosan solution prior to mixing. To better understand the role of electrostatics, we also explored encapsulation of the protein lysozyme which bears a net positive charge (isoelectric point ~ 11). Alexa Fluor 647 labeled lysozyme was also localized in the outermost region of the gel, whether the protein was dissolved in the PA solution or the chitosan solution, as shown by the confocal microscopy (Fig. 6C and 6D). The fluorescence intensity line cuts (Fig. 6E-H) show high density of both chitosan and PA on the outermost region of the gel sheets as a result of their

complexation. This dense region acts as a diffusion barrier that can trap proteins regardless of their charge.

Conclusions

We have shown that mixing of a supramolecular polymer with a polyelectrolyte of opposite charge leads to rapid formation of a hydrogel containing crumpled sheets, and the complexation at the interfaces of the mixing solutions leads to nonequilibrium structures with distinct domains. Interestingly, decreasing concentrations of the supramolecular polymer were found to lower the solution viscosity, allowing greater complexation during mixing, resulting in gels with higher shear moduli. The hydrogels have tunable rheological properties and the ability to encapsulate and retain proteins. The formation of a dense contact layer at the interface of the supramolecular polymer and polyelectrolyte during gelation localizes both positively and negatively charged proteins in the outermost layer of the gel. These gels, with their tunable mechanical properties and the ability to encapsulate proteins, could be useful biomaterials for protein delivery in regenerative medicine and wound healing.

Experimental

Gelation: Unless otherwise noted, equal volumes of PA and chitosan solutions were injected into opposite sides of a 20 mL scintillation vial. The solutions were then immediately vortex mixed together for ten seconds on the highest mixing setting of a Scientific Industries Vortex Genie.

Scanning Electron Microscopy: Gels were placed into microporous specimen capsules (Electron Microscopy Sciences) and solvent exchanged into absolute ethanol by placing the capsule into 30%, 40%, 50%, 60%, 70%, 80%, 90%, 95% ethanol-water solutions for 10 minutes, followed by 15 minutes in a 100% ethanol solution. Following solvent exchange into absolute ethanol, the gel was critical point dried in the specimen capsule using a Tousimis Samdri-795 Critical Point Dryer. The dry gel was then coated with 10 nm of osmium using a Filgen Osmium Plasma Coater OPC60A, and micrographs were taken using a Hitachi S-4800 scanning electron microscope.

Solution Rheology: Viscosity measurements were performed using an Anton Paar MCR 302 Rheometer. The CP50-1 fixture (50 mm cone with 1° angle) was used to measure viscosity of 600 μ L solutions (25 °C). Mean viscosities were calculated at each shear rate by averaging the measured viscosities in a 100 second interval after the experiment reached steady state.

Rheology of E3OH-Chitosan Gels: Measurements were performed using an Anton Paar MCR 302 Rheometer. The PP20 fixture (20 mm plate) was used with a normal force gap setting of 0.1 N and a temperature of 25 °C. Gels were solvent exchanged in deionized water for 24 hours prior to testing to ensure that all gels remained at the same pH and ionic strength. Amplitude sweeps were performed using a logarithmic ramp from 0.01% strain to 100% strain with constant frequency of 10 rad/s.

X-ray Scattering: X-ray scattering experiments were performed at Beamline 5-ID-D, DND-CAT, Advanced Photon Source at the Argonne National Laboratory. An X-ray energy of 17 keV was selected using a double monochromator, and the scattering patterns for an empty cell, water-filled cell and sample-filled cell were recorded using a set of three charge coupled device (CCD) detectors.⁵⁴ The hydrogel samples were sealed in Grace Bio-Labs silicone isolators with

Chemplex 7.5 μm Kapton windows and placed in the beam. The solution samples were placed in a vacuum flow cell comprising of a 1.5 mm quartz capillary connected to a syringe pump. The two-dimensional scattering patterns then azimuthally integrated to generate a scattering vector magnitude q vs. intensity plot, where q is defined as $q=4\pi\sin(\theta)/\lambda$ for which θ denotes the half of total scattering angle and λ the X-ray wavelength, 0.7293 Å. 2D to 1D data reduction was performed by GSAS-II software.⁵⁵ We did not attempt to determine the absolute scattering intensity.

Confocal Microscopy: Gels were placed on a glass slide with an adhesive spacer that was then covered with cover glass. Imaging was performed on the Leica SP5 Confocal Microscope and the Nikon A1R Confocal Microscope. On the Leica SP5 Confocal Microscope, the 488 nm laser line was used to image the FITC-Chitosan and the 543 nm laser line to image the TAMRA-E3. On the Nikon A1R Confocal Microscope, the 488 nm laser line was used to image the FITC-Chitosan and the 561 nm laser line to image the TAMRA-E3, and the 640 nm laser line to image the Alexa Fluor 647-labeled BSA and Alexa Fluor 647-labeled lysozyme.

Author contributions

T.J.C. designed and performed experiments, analyzed data, and wrote the manuscript. H.S. and C.P. performed experiments, analyzed data, and provided helpful discussion. L.C.P. provided helpful discussion and wrote the manuscript. S.I.S wrote the manuscript and supervised this research.

Conflicts of interest

There are no conflicts to declare.

Acknowledgements

This work was primarily supported by the Center for Bio-Inspired Energy Science, an Energy Frontier Research Center funded by the U.S. Department of Energy, Office of Science, Basic Energy Sciences under Award # DE-SC0000989 (peptide amphiphile synthesis and purification, confocal microscopy, scanning electron microscopy, rheology, transmission electron microscopy, absorbance spectroscopy). This work was also supported by the Nanyang Technological University-Northwestern Institute of Nanomedicine (protein release studies). T.J.C. was supported by NSF GRFP grant number DGE-1842165. X-ray diffraction was performed at the DuPont-Northwestern-Dow Collaborative Access Team (DNDCAT) located at Sector 5 of the Advanced Photon Source (APS). DND-CAT is supported by Northwestern University, E.I. DuPont de Nemours & Co., and The Dow Chemical Company. This research used resources of the Advanced Photon Source, a U.S. Department of Energy (DOE) Office of Science User Facility operated for the DOE Office of Science by Argonne National Laboratory under Contract No. DE-AC02-06CH11357. The X-ray scattering data was collected using an instrument funded by the National Science Foundation under Award Number 0960140. This work used the following core facilities at Northwestern University: the Peptide Synthesis Core Facility and the Analytical BioNanoTechnology Equipment Core facility (ANTEC) of the Simpson Querrey Institute for peptide synthesis and purification as well as rheometry, the EPIC facility of Northwestern's NUANCE Center for SEM and TEM, the Materials Characterization and Imaging Facility (MatCI) for rheometry, and the Biological Imaging Facility (BIF) for confocal microscopy. The EPIC facility of Northwestern University's NUANCE Center has received support from the Soft and Hybrid Nanotechnology Experimental (SHyNE) Resource (NSF ECCS-1542205); the MRSEC program (NSF DMR-1720139) at the Materials Research Center; the International Institute for Nanotechnology (IIN); the Keck Foundation; and the State

of Illinois, through the IIN. ANTEC is also currently supported by the SHyNE Resource (NSFECCS-1542205). The Simpson Querrey Institute, Northwestern University Office for Research, U.S. Army Research Office, and the U.S. Army Medical Research and Materiel Command have also provided funding to develop this facility. The authors thank M. Seniw for the preparation of molecular illustrations and J. Passarelli for review of the manuscript.

References

- 1 S. Srivastava and M. V. Tirrell, *Adv. Chem. Phys.*, 2016, **161**, 499–544.
- 2 G. Decher, *Science*, 1997, **277**, 1232–1237.
- 3 N. J. Shah, M. L. Macdonald, Y. M. Beben, R. F. Padera, R. E. Samuel and P. T. Hammond, *Biomaterials*, 2011, **32**, 6183–6193.
- 4 H. Cui, N. Pan, W. Fan, C. Liu, Y. Li, Y. Xia and K. Sui, *Adv. Funct. Mater.*, 2019, **29**, 1807692.
- 5 C. H. Kuo, L. Leon, E. J. Chung, R. T. Huang, T. J. Sontag, C. A. Reardon, G. S. Getz, M. V. Tirrell and Y. Fang, *J. Mater. Chem. B*, 2014, **2**, 8142–8153.
- 6 I. K. Voets, A. de Keizer and M. A. Cohen Stuart, *Adv. Colloid Interface Sci.*, 2009, **147–148**, 300–318.
- 7 S. Srivastava, M. Andreev, A. E. Levi, D. J. Goldfeld, J. Mao, W. T. Heller, V. M. Prabhu, J. J. de Pablo and M. V. Tirrell, *Nat. Commun.*, 2017, **8**, 14131.
- 8 J. N. Hunt, K. E. Feldman, N. A. Lynd, J. Deek, L. M. Campos, J. M. Spruell, B. M. Hernandez, E. J. Kramer and C. J. Hawker, *Adv. Mater.*, 2011, **23**, 2327–2331.
- 9 J. T. Overbeek and M. J. Voorn, *J. Cell. Physiol. Suppl.*, 1957, **49**, 7–22.
- 10 Q. Wang and J. B. Schlenoff, *Macromolecules*, 2014, **47**, 3108–3116.
- 11 C. P. Brangwynne, P. Tompa and R. V. Pappu, *Nat. Phys.*, 2015, **11**, 899–904.
- 12 S. F. Banani, H. O. Lee, A. A. Hyman and M. K. Rosen, *Nat. Rev. Mol. Cell Biol.*, 2017, **18**, 285–298.
- 13 M. Matsusaki, K. Sakaue, K. Kadowaki and M. Akashi, *Adv. Healthc. Mater.*, 2013, **2**, 534–539.
- 14 J. Wang, Y. F. Xue, X. C. Chen, M. Hu, K. F. Ren and J. Ji, *Adv. Healthc. Mater.*, 2020, **9**, 1–10.
- 15 A. L. Rutz, K. E. Hyland, A. E. Jakus, W. R. Burghardt and R. N. Shah, *Adv. Mater.*, 2015, **27**, 1607–1614.
- 16 X. C. Chen, K. F. Ren, J. H. Zhang, D. D. Li, E. Zhao, Z. J. Zhao, Z. K. Xu and J. Ji, *Adv. Funct. Mater.*, 2015, **25**, 7470–7477.
- 17 C. L. Silva, J. C. Pereira, A. Ramalho, A. A. C. C. Pais and J. J. S. Sousa, *J. Memb. Sci.*, 2008, **320**, 268–279.
- 18 J. B. Matson and S. I. Stupp, *Chem. Commun.*, 2012, **48**, 26–33.
- 19 M. J. Webber, E. A. Appel, E. W. Meijer and R. Langer, *Nat. Mater.*, 2015, **15**, 13–26.
- 20 M. J. Webber and R. Langer, *Chem. Soc. Rev.*, 2017, **46**, 6600–6620.
- 21 X. Sun and T. D. James, *Chem. Rev.*, 2015, **115**, 8001–8037.

- 22 M. P. Hendricks, K. Sato, L. C. Palmer and S. I. Stupp, *Acc. Chem. Res.*, 2017, **50**, 2440–2448.
- 23 J. D. Hartgerink, E. Beniash and S. I. Stupp, *Science*, 2001, **294**, 1684–1688.
- 24 P. Berndt, G. B. Fields and M. V. Tirrell, *J. Am. Chem. Soc.*, 1995, **117**, 9515–9522.
- 25 J. D. Hartgerink, E. Beniash and S. I. Stupp, *Proc. Natl. Acad. Sci.*, 2002, **99**, 5133–5138.
- 26 C. J. Newcomb, S. Sur, J. H. Ortony, O. S. Lee, J. B. Matson, J. Boekhoven, J. M. Yu, G. C. Schatz and S. I. Stupp, *Nat. Commun.*, 2014, **5**, 1–10.
- 27 F. Tantakitti, J. Boekhoven, X. Wang, R. V. Kazantsev, T. Yu, J. Li, E. Zhuang, R. Zandi, J. H. Ortony, C. J. Newcomb, L. C. Palmer, G. S. Shekhawat, M. Olvera de la Cruz, G. C. Schatz and S. I. Stupp, *Nat. Mater.*, 2016, **15**, 469–476.
- 28 J. H. Ortony, C. J. Newcomb, J. B. Matson, L. C. Palmer, P. E. Doan, B. M. Hoffman and S. I. Stupp, *Nat. Mater.*, 2014, **13**, 812–816.
- 29 S. S. Lee, E. L. Hsu, M. Mendoza, J. Ghodasra, M. S. Nickoli, A. Ashtekar, M. Polavarapu, J. Babu, R. M. Riaz, J. D. Nicolas, D. Nelson, S. Z. Hashmi, S. R. Kaltz, J. S. Earhart, B. R. Merk, J. S. Mckee, S. F. Bairstow, R. N. Shah, W. K. Hsu and S. I. Stupp, *Adv. Healthc. Mater.*, 2015, **4**, 131–141.
- 30 S. S. Lee, T. Fyrner, F. Chen, Z. Álvarez, E. Sleep, D. S. Chun, J. A. Weiner, R. W. Cook, R. D. Freshman, M. S. Schallmo, K. M. Katchko, A. D. Schneider, J. T. Smith, C. Yun, G. Singh, S. Z. Hashmi, M. T. McClendon, Z. Yu, S. R. Stock, W. K. Hsu, E. L. Hsu and S. I. Stupp, *Nat. Nanotechnol.*, 2017, **12**, 821–829.
- 31 J. C. Stendahl, M. S. Rao, M. O. Guler and S. I. Stupp, *Adv. Funct. Mater.*, 2006, **16**, 499–508.
- 32 M. A. Greenfield, J. R. Hoffman, M. Olvera de la Cruz and S. I. Stupp, *Langmuir*, 2010, **26**, 3641–3647.
- 33 J. M. Godbe, R. Freeman, L. F. Burbulla, J. Lewis, D. Krainc and S. I. Stupp, *ACS Biomater. Sci. Eng.*, 2020, **6**, 1196–1207.
- 34 R. M. Capito, H. S. Azevedo, Y. S. Velichko, A. Mata and S. I. Stupp, *Science*, 2008, 1812–1816.
- 35 D. Carvajal, R. Bitton, J. R. Mantei, Y. S. Velichko, I. Stupp and K. R. Shull, *Soft Matter*, 2010, **6**, 1816–1823.
- 36 Y. S. Velichko, J. R. Mantei, R. Bitton, D. Carvajal, K. R. Shull and S. I. Stupp, *Adv. Funct. Mater.*, 2012, **22**, 369–377.
- 37 R. H. Zha, S. Sur and S. I. Stupp, *Adv. Healthc. Mater.*, 2013, **2**, 126–133.
- 38 L. W. Chow, R. Bitton, M. J. Webber, D. Carvajal, K. R. Shull, A. K. Sharma and S. I. Stupp, *Biomaterials*, 2011, **32**, 1574–1582.
- 39 J. Borges, M. P. Sousa, G. Cinar, S. G. Caridade, M. O. Guler and J. F. Mano, *Adv. Funct. Mater.*, 2017, 1605122.
- 40 E. Radvar and H. S. Azevedo, *ACS Biomater. Sci. Eng.*, 2019, **5**, 4646–4656.
- 41 C. L. Hedegaard, E. C. Collin, C. Redondo-Gómez, L. T. H. Nguyen, K. W. Ng, A. A. Castrejón-Pita, J. R. Castrejón-Pita and A. Mata, *Adv. Funct. Mater.*, 2018, **28**, 1–13.
- 42 K. E. Inostroza-Brito, E. Collin, O. Siton-Mendelson, K. H. Smith, A. Monge-Marcet, D. S. Ferreira, R. P. Rodríguez, M. Alonso, J. C. Rodríguez-Cabello, R. L. Reis, F. Sagués, L. Botto, R. Bitton, H. S. Azevedo and A. Mata, *Nat. Chem.*, 2015, **7**, 897–904.
- 43 T. Vermonden, R. Censi and W. E. Hennink, *Chem. Rev.*, 2012, **112**, 2853–2888.
- 44 J. Li and D. J. Mooney, *Nat. Rev. Mater.*, 2016, **1**, 16071.
- 45 K. Murakami, H. Aoki, S. Nakamura, S. ichiro Nakamura, M. Takikawa, M. Hanzawa, S.

- Kishimoto, H. Hattori, Y. Tanaka, T. Kiyosawa, Y. Sato and M. Ishihara, *Biomaterials*, 2010, **31**, 83–90.
- 46 R. Jayakumar, M. Prabakaran, P. T. Sudheesh Kumar, S. V. Nair and H. Tamura, *Biotechnol. Adv.*, 2011, **29**, 322–337.
- 47 J. M. Ottino, *The Kinematics of Mixing: stretching, chaos, and transport*, Cambridge University Press, Cambridge, 1989.
- 48 D. M. Hobbs and F. J. Muzzio, *Chem. Eng. J.*, 1997, **67**, 153–166.
- 49 S. Wiggins and J. M. Ottino, *Philosophical Trans. R. Soc. A*, 2004, **362**, 937–970.
- 50 T. J. Moyer, J. A. Finbloom, F. Chen, D. J. Toft, V. L. Cryns and S. I. Stupp, *J. Am. Chem. Soc.*, 2014, **136**, 14746–14752.
- 51 S. Tsonchev, K. L. Niece, G. C. Schatz, M. A. Ratner and S. I. Stupp, *J. Phys. Chem. B*, 2008, **112**, 441–447.
- 52 J. E. Goldberger, E. J. Berns, R. Bitton, C. J. Newcomb and S. I. Stupp, *Angew. Chemie*, 2011, **123**, 6416–6419.
- 53 R. H. Zha, Y. S. Velichko, R. Bitton and S. I. Stupp, *Soft Matter*, 2016, **12**, 1401–1410.
- 54 S. J. Weigand and D. T. Keane, *Nucl. Inst. Methods Phys. Res. A*, 2011, **649**, 61–63.
- 55 B. H. Toby and R. B. Von Dreele, *J. Appl. Crystallogr.*, 2013, **46**, 544–549.